JOURNAL OF SOLID STATE CHEMISTRY 112, 381–386 (1994)

The Role of Ti^{4+} on the Structure and Transformations of Gel-Produced Zn_2SiO_4

Chung-Cherng Lin and Pouyan Shen[1]

Institute of Materials Science and Engineering, National Sun Yat-Sen University, Kaohsiung, Taiwan 804, Republic of China

Received June 30, 1993; in revised form November 29, 1993; accepted December 2, 1993

The structure and nonisothermal transformations of gel-produced Zn_2SiO_4 containing a minor amount (5 mole%) of TiO_2 precursor (titanium *n*-propoxide) were studied. Evidence from infrared and Raman spectroscopy indicated that the dissolved Ti^{4+} enhanced the formation of silicate clusters. On the other hand, Ti^{4+} became tetrahedrally coordinated when the gel transformed into the β and subsequently the α phase. The presence of Ti^{4+} lowered the onset and peak temperatures of the transformation in the differential thermal analysis but increased the apparent activation energy for both the crystallization and the $\beta \rightarrow \alpha$ transformation. Ti^{4+} also resulted in early site saturation for crystallization and slightly delayed site saturation in the subsequent $\beta \rightarrow \alpha$ transformation. This can be accounted for by the effect of Ti^{4+} on the number of bulk nucleation sites, viz. SiO_4 in the gel and TiO_4 or lattice imperfections in the β phase.

1. INTRODUCTION

TiO_2 has been used as nucleant in a number of glass–ceramic systems, e.g., SiO_2–Al_2O_3–MgO (1, 2), Li_2O–Al_2O_3–SiO_2 (3); Al_2O_3–SiO_2–ZnO (4); and MgO–ZnO–SiO_2 (5). The effects of TiO_2 on phase transformation of Zn_2SiO_4 have also been investigated by a few authors. TiO_2 acts as a catalyst in the SiO_2–ZnO reaction to form willemite (α-Zn_2SiO_4) (6). On the other hand TiO_2 addition to SiO_2–ZnO melts retained the metastable phase β-Zn_2SiO_4 to room temperature, i.e., suppressed the $\beta \rightarrow \alpha$-Zn_2SiO_4 transformation (6). It has also been suggested from optical microscopy that TiO_2 inhibits the crystallization of willemite from spodumene–willemite–diopside glasses (7). This research shows further that the effect of TiO_2 on the transformation differs in an amorphous and crystalline Zn_2SiO_4, the cause being the dependence of nucleation sites on the parent structure.

Ti^{4+} predominantly enters tetrahedral site in the high silica region but octahedral site in the low silica region for $K_2O \cdot SiO_2 \cdot TiO_2$ glasses (8). Other works suggested tetrahedral coordination of Ti^{4+} in silicate glasses of various composition systems, e.g., K_2O–SiO_2–TiO_2 (9), $Li_2Si_2O_5$–TiO_2 (10), and $K_2O \cdot 2TiO_2$ (11). Willemite (α-Zn_2SiO_4) also forms solid solution with TiO_2 (6) by substituting Ti^{4+} for Si^{4+} with tetrahedral coordination (12, 13). However, the structures of Ti^{4+} – bearing polymorphs of Zn_2SiO_4, which are important to the understanding of the role of Ti^{4+} in the crystallization of β phase and $\beta \rightarrow \alpha$ transition, need to be clarified.

In our previous paper, Zn_2SiO_4 was synthesized via a sol–gel route using organometallic compounds as precursors (14). The effect of the hydrolysis condition on the gel synthesis and subsequent transformations (14) and the mechanism of both transformations (15) were also studied. This research further studies if the structure of the Zn_2SiO_4 polymorphs and their transformation kinetics are affected by the addition of TiO_2 precursor during synthesis.

2. EXPERIMENTAL

Procedure for the sol–gel synthesis of amorphous Zn_2SiO_4 sample is the same as that for sample ZS_1 in the previous paper (14). To prepare the TiO_2-bearing (5 mole%) sample ZST, *t*-BuOH solution of titanium *n*-propoxide ($Ti(n\text{-}OPr)_4$) was added to ZS_1 precursor before the second-stage synthesis (base-catalyzed hydrolysis and condensation) and after the addition of diethylzinc. Nonisothermal DTA and thermogravimetric analysis (TGA) (at a heating rate of 2.5, 5, 7.5, and 10°C/min) and the equation of Matusita *et al.* (16) were used to study transformation kinetics as adopted in previous papers (15). FTIR and Raman spectroscopy under the same conditions as those employed by Lin and Shen (14) were used to study the gel structure and their polymorphs after heat treatments. Other compounds such as amorphous TiO_2 and α-Zn_2TiO_4 synthesized from the same precursors were used as reference materials for vibrational spectroscopy.

[1] To whom correspondence should be addressed.

0022-4596/94 $6.00

TABLE 1
Phases Detected by XRD before or after DTA Runs

Sample	Raw materials	As-formed	600°C	800°C	1000°C
ZS_1	TEOS + $ZnEt_2$	a	a	β	α
ZST	TEOS + $ZnEt_2$ + $Ti(OPr)_4$	a	a	β	α

Note. DTA conducted at 10°C/min. a, amorphous; α, α-Zn_2SiO_4; β, β – Zn_2SiO_4; TEOS, tetraethyl orthosilicate; $ZnEt_2$, diethylzinc; $Ti(OPr)_4$, titanium *n*-propoxide.

3. RESULTS AND DISCUSSION

The phases identified by X-ray diffraction (XRD, Cu$K\alpha$) from the as-formed or calcined ZS_1 and ZST samples are listed in Table 1. The as-formed powders of both compositions are amorphous and survived heating above 600°C before transformation into β and then α phases. Figure 1 gives the representative DTA traces of gel-produced ZS_1 and ZST powders by which the kinetics of transformations were evaluated. According to transmission electron microscopy observations (not shown in this paper), the as-formed powders of sample ZST have nearly the same particle size as sample ZS_1. Sharp exothermic peaks appeared during crystallization of β phase and $\beta \rightarrow \alpha$ transition for both ZS_1 and ZST samples. In the following, the structures and transformation kinetics of gel-produced ZST are compared to those of ZS_1.

3.1. Vibrational Spectroscopy

Figure 2 and Figure 3 show, respectively, the infrared spectra of as-formed samples ZS_1 and ZST and their polymorphs after thermal evolution (note that the absorption

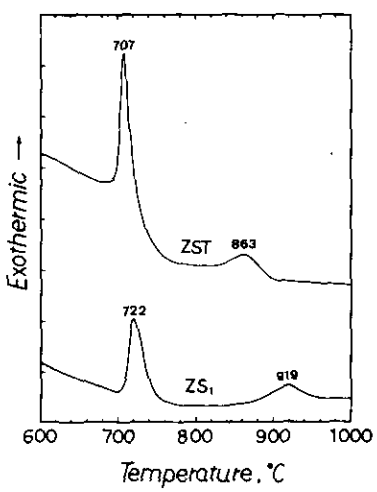

FIG. 1. DTA traces of samples ZS_1 (Zn_2SiO_4) and ZST (Ti^{4+}-bearing Zn_2SiO_4). The numerical values are the peak temperatures (full scale is 40 μV and heating rate is 10 K/min).

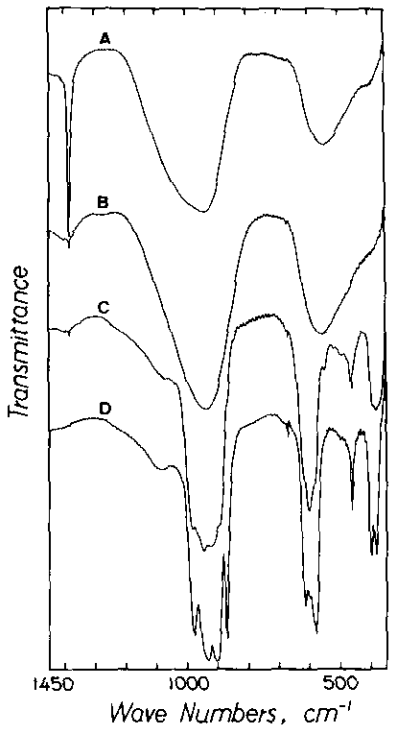

FIG. 2. FTIR spectra of sample ZS_1 after thermal evolution. (A) As-formed (amorphous) and (B, C, and D) amorphous, β phase, and α phase after DTA runs up to 600, 800, and 1000°C, respectively, after Lin and Shen (14).

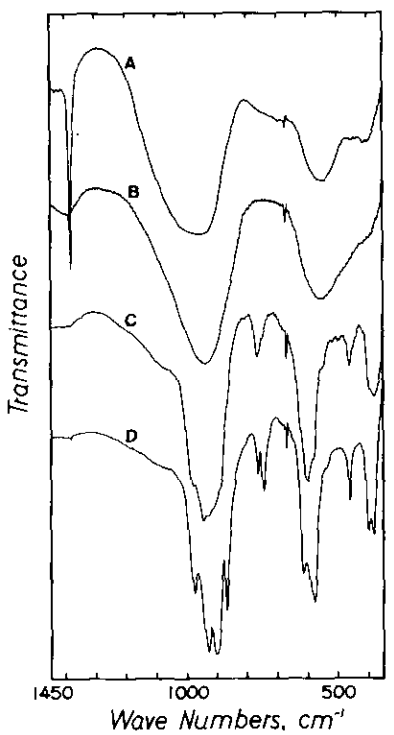

FIG. 3. FTIR spectra of sample ZST. (A) As-formed (amorphous) and (B, C, and D) amorphous, β phase, and α phase after DTA runs up to 600, 800, and 1000°C, respectively.

at about 660 cm^{-1} is not the characteristic band of sample, but resulted from the inherent noise after the background was subtracted from the spectra). Table 2 lists infrared absorptions of reference materials including anatase and rutile which have Ti^{4+} in coordination number of 6 (10, 17). The characteristic IR bands of various TiO_2 polymorphs did not appear for specimen ZST before or after thermal exposure, suggesting that the solid solution of TiO_2 in the polymorphs of Zn_2SiO_4 is nearly complete. The spectra of gel-produced Zn_2SiO_4 in samples ZST are basically the same as ZS_1 except the doublet for crystalline phases β (750 and 768 cm^{-1}) and α (747 and 764 cm^{-1}) (spectra C and D in Fig. 3) is unique to ZST samples. The presence of this doublet suggests that the coordination of Ti^{4+} in α and β phase is tetrahedral analogous to TiO_4 (Table 2; refer also to Refs. 12, 18).

The effect of Ti^{4+} on the structure of a gel which cannot be discerned clearly on FTIR is revealed by Raman spectroscopy in Fig. 4A. In contrast to specimen ZS_1 (14), the spectrum of as-formed ZST gel shows a strong Raman scattering centered at 1056 cm^{-1} besides a broad scattering centered at 924 cm^{-1} as in ZS_1. This extra band belongs to the Si_2O_5 unit (19–21) rather than the TiO_4 or TiO_6 polyhedron, which has a far lower frequency of Raman scattering. Therefore the addition of Ti^{4+} during synthesis caused clusters of silicate units which may then influence the crystallization and $\beta \rightarrow \alpha$ transition kinetics as shown in the next section. Note that the $(Si_2O_5)_n$ sheets or more polymerized units also exist in $Li_2O \cdot 2SiO_2 \cdot xTiO_2$ silicate glasses in the range of $0.3 \leq x \leq 1.0$ and the TiO_4 incorporated into $(Si_2O_5)_n$ sheets exists as network former (10). The polymerizing role of Ti^{4+} in the silicate melts has also been indicated (22).

TABLE 2
Infrared Absorptions of TiO_2-Bearing Phases Relevant Possibly to the Structure of Ti^{4+}-Bearing Zn_2SiO_4

Phase	IR absorption, cm^{-1}	References
amorphous TiO_2	780 b, 545 sb, 420 sb	This work
Anatase	700 s vb, 608 s vb, 347 m	McDevitt and Baun (27)
Rutile	695 sb, 608 sb, 423 w, 352 w	
$ZnTiO_3$	590 b, 400, 315 sh	Last (28)
α-Zn_2TiO_4	695 w sh, 525w sh, 580 s vb, 425 sb	This work
α-$Zn_2(Si, Ti)O_4$ (TiO_2 = 1 ~ 10 mol%)	765, 747, and 320 other absorptions are identical to willemite	Tarte (12)
TiO_4	650–800	Tarte (12, 18)
TiO_6	400–500	

Note. b, broad; s, strong; vb, very broad; m, moderate; sh, shoulder; w, weak.

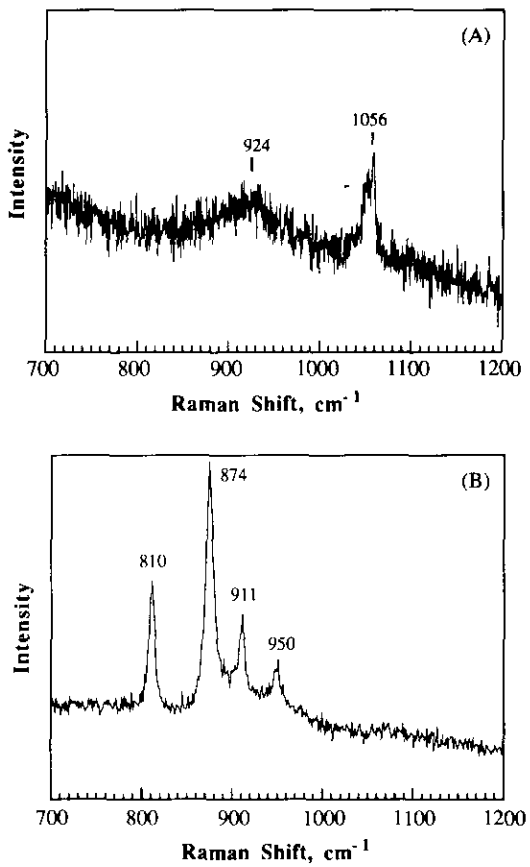

FIG. 4. Raman spectra of sample ZST. (A) As-formed (amorphous) and (B) α phase (after DTA run up to 1000°C).

The Raman spectra of amorphous phase and β phase of sample ZST cooled from 600 and 700°C, respectively, are not shown in this paper. This is because the strong fluorescence background shields characteristic bands, if any, of the polymorphs. Thus both FTIR and Raman spectroscopy failed to detect the Ti^{4+}-occupied polyhedra in amorphous Zn_2SiO_4. Removing organic groups during heating was probably difficult with sample ZST than sample ZS_1, as the latter appeared to have less fluorescence background on Raman spectra upon thermal evolution (14). The α phase in specimen ZST (Fig. 4B) has the same Raman bands as obtained in ZS_1 (14), except for an extra Raman shift at 810 cm^{-1} which can be attributed to the strained TiO_4 analogous to that in $K_2O \cdot TiO_2$ and $Cs_2O \cdot TiO_2$ (23). Note that a strained polyhedra may cause Raman shift to a higher wave number as indicated by the pressure dependence of Raman shift for TiO_2 (24).

3.2. *Kinetics of Transformations*

The DTA onset and peak temperatures for crystallization of β phase and $\beta \rightarrow \alpha$ transition were lowered by the presence of Ti^{4+} (Fig. 1 and Table 3). Since the bond strength of Ti–O is lower than that of Si–O as indicated

TABLE 3
DTA Onset and Peak Temperatures for Samples ZS_1 and ZST (Heating Rate = 10°C/min)

	Transition			
	Crystallization (°C)		$\beta \rightarrow \alpha$ transition (°C)	
Sample	T_o	T_p	T_o	T_p
ZS_1	709	722	876	918.6
ZST	696	707.4	821	863

Note. ZS_1, Zn_2SiO_4; ZST, Zn_2SiO_4 dissolved with 5 mol% TiO_2; T_o, onset temperature; T_p, peak temperature.

by vibrational spectroscopy, a low viscosity or high diffusivity is expected to lower the crystallization temperature for sample ZST. The exothermal peak for $\beta \rightarrow \alpha$ transition in sample ZST is also affected by TiO_4, which increases nucleation sites as discussed below.

Similar to sample ZS_1 (refer to Lin and Shen (15)), the slope of the $\ln[-\ln(1-x)]$ vs $\ln \phi$ plot (i.e., $-n$ values) of sample ZST decreases with increasing temperature for

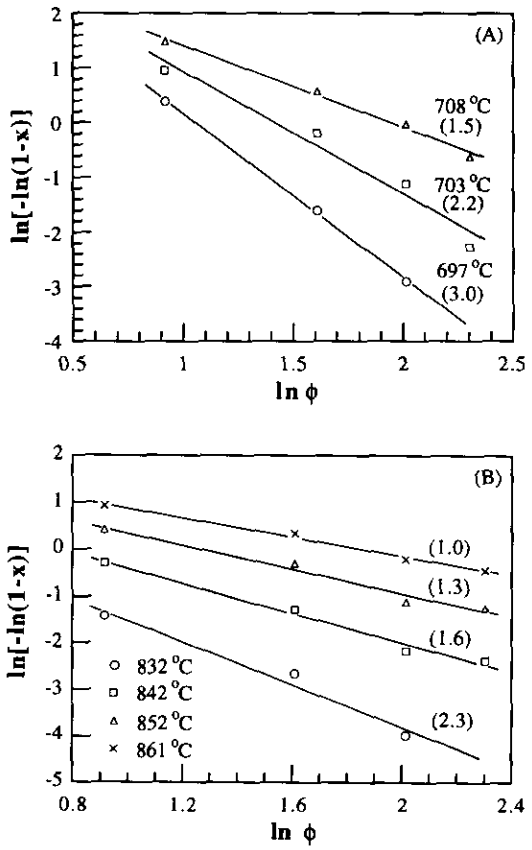

FIG. 5. $\ln[-\ln(1-x)]$ vs $\ln \phi$ plot for (A) crystallization and (B) $\beta \rightarrow \alpha$ transition of sample ZST; negative slopes (i.e., n values) are given in parentheses.

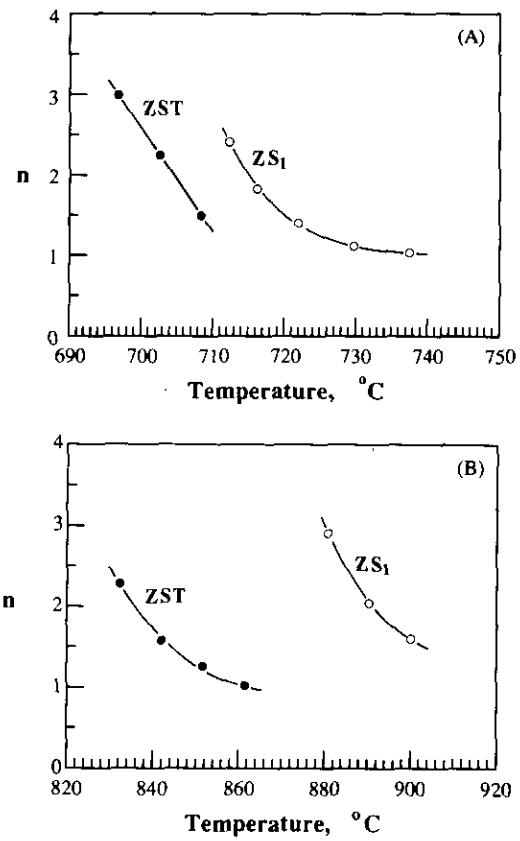

FIG. 6. Variation of n values with the change of temperature for (A) crystallization of β phase and (B) $\beta \rightarrow \alpha$ transformation of samples ZS_1 and ZST.

both crystallization of β phase and $\beta \rightarrow \alpha$ transformation (Fig. 5). The variation of n values with the change of temperature in crystallization and $\beta \rightarrow \alpha$ transformation for ZS_1 and ZST is plotted in Fig. 6. Analogous to sample ZS_1 (15), the temperature dependence of n values for sample ZST is attributed mainly to site saturation at bulk nucleation sites followed by one-dimensional growth. It is noted that the $\ln[-\ln(1-x)]$ vs $1/T$ plot has a slope break at $x \approx 0.45$ for crystallization of β phase and $x \approx 0.36$ for $\beta \rightarrow \alpha$ transition in sample ZST (Fig. 7). The corresponding slope breaks appear at $x \approx 0.63$ and 0.30, respectively, for sample ZS_1 (15); i.e., the Ti^{4+}-bearing sample tends to reach early site saturation for crystallization of β phase but slightly late site saturation for $\beta \rightarrow \alpha$ transition. This cannot be attributed to the change in the number of surface nucleation sites because sample ZST has proximate size to ZS_1. Instead, we suggest that the change in x values for the two transformations is due to the fact that the Ti^{4+} lowers the number of SiO_4 units (due to the formation of Si_2O_5) in the gel but creates TiO_4 units or the related lattice imperfections in the β phase which likely act as bulk nucleation sites in these phases.

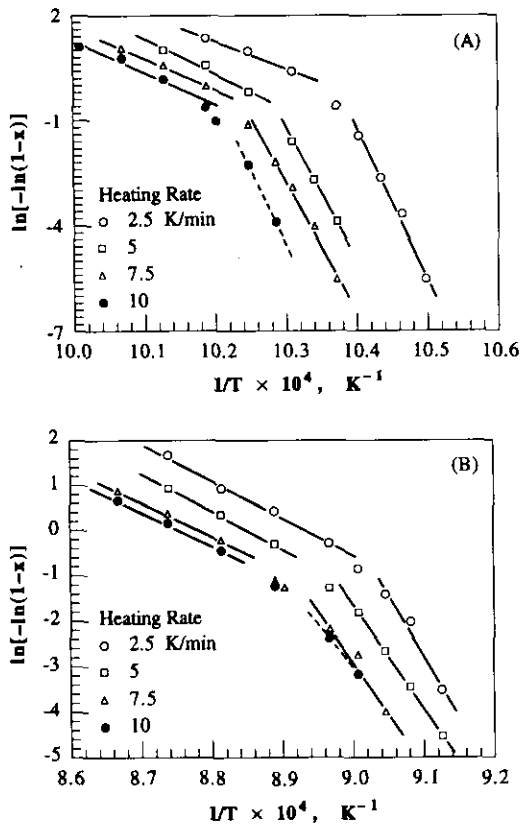

FIG. 7. $\ln[-\ln(1-x)]$ vs $1/T$ plot for (A) crystallization and (B) $\beta \rightarrow \alpha$ transition of sample ZST.

Thus the dependence of nucleation sites on parent structure may account for the diverse effect of TiO_2 on the transformation in an amorphous matrix (e.g., the crystallization of Zn_2SiO_4 in the gel or silicate glass (7)) vs crystalline matrix (e.g., the $\beta \rightarrow \alpha$ transition of Zn_2SiO_4 (6)). It remains to be studied if this consideration can be extended to the coordination effect of TiO_2 (25) on the devitrification and subsequent transformation in various glasses.

The slope of the $\ln[-\ln(1-x)]$ vs $1/T$ plot is steeper (i.e., higher activation energy) for sample ZST than ZS_1 (refer to Lin and Shen (15)) both in crystallization of β phase and in $\beta \rightarrow \alpha$ transition. In order to extend the Si–O–Zn linkage or diffusion in a gel-produced material, some of the Ti–O and Si–O–Si (in the Si_2O_5 unit) bonds probably must be broken and therefore a higher activation energy results even though TiO_4 plays the role of nucleant in the $\beta \rightarrow \alpha$ transition. A nucleant-promoted lowering in crystallization temperature but not in activation energy for crystal growth has also been reported in some melt-derived glasses (e.g., devitrification of $Li_2O \cdot 2SiO_2$ glass with addition of Ag_2O (26)) although the mechanism may not be the same as that in gel-derived materials. It is noteworthy that the activation energy of willemite formation was reduced by TiO_2 addition to the $ZnO–SiO_2$ powder mixture (6). This is due to the fact that TiO_2 acts as a catalyst in the reaction, a parabolic one involving the diffusion of Zn^{2+} and Si^{4+} to the product sites (6).

4. CONCLUSIONS

1. Addition of TiO_2 using titanium *n*-propoxide during synthesis of Zn_2SiO_4 enhanced the clustering of slicate units in the gel.

2. The DTA onset and peak temperatures for cystallization of β phase and $\beta \rightarrow \alpha$ transition were lowered due to the substitution of Ti^{4+} ion in the silicate network.

3. In the lattices of α- and β-Zn_2SiO_4, Ti^{4+} has tetrahedral coordination.

4. The dependence of nucleation sites and mass transport on parent structure may possibly account for the diverse effect of TiO_2 on the transformation in an amorphous vs crystalline matrix. It remains to be studied if this consideration can be extended to the coordination effect of TiO_2 on devitrification and subsequent transformation in various glasses.

ACKNOWLEDGMENT

We thank an anonymous referee for helpful comments.

REFERENCES

1. A. G. Gregory and T. J. Veasey, *J. Mater. Sci.* **6,** 1312 (1971).
2. T. I. Barry, J. M. Cox, and R. Morrell, *J. Mater. Sci.* **13,** 594 (1978).
3. G. Partridge, *Glass Technol.* **23,** 133 (1982).
4. Y. Shan, J. Li, Z. Deng, and X. Zhou, *J. Non-Cryst. Solids* **52,** 275 (1982).
5. Z. X. Chen and P. W. McMillan, *J. Mater. Sci.* **20,** 3428 (1985).
6. C. C. Lee, P. Shen, and H. Y. Lu, *J. Mater. Sci.* **24,** 3300 (1989).
7. A. W. A. El-Shennawi, A. A. Omar, and A. M. Morsy, *Thermochim. Acta* **58,** 125 (1982).
8. Bh. V. J. Rao, *Phys. Chem. Glasses* **4,** 22 (1963).
9. N. Iwamoto, Y. Tsunawaki, M. Fuji, and T. Hartfori, *J. Non-Cryst. Solids* **18,** 303 (1975).
10. T. Furukawa and W. B. White, *Phys. Chem. Glasses* **20,** 69 (1979).
11. S. Sakka, F. Miyaji, and K. Fukumi, *J. Non-Cryst. Solids* **107,** 171 (1989).
12. P. Tarte, *Nature* **191,** 1002 (1961).
13. D. Ganguli, *Neues Jahrb. Miner. Abh.* **123,** 313 (1975).
14. C. C. Lin and P. Shen, *J. Non-Cryst. Solids*, in press (1994).
15. C. C. Lin and P. Shen, *J. Solid State Chem.*, in press (1994).
16. K. Matusita, T. Komatsu, and R. Yokota, *J. Mater. Sci.* **19,** 291 (1984).
17. W. B. White and R. Roy. *Am. Mineral.* **49,** 1670 (1964).
18. P. Tarte, *Spectrochim. Acta* **18,** 467 (1962).
19. T. Furukawa, K. E. Fox, and W. B. White, *J. Chem. Phys.* **75,** 3226 (1981).
20. B. O. Mysen, D. Virgo, and C. M. Scarfe, *Am. Mineral.* **65,** 690 (1980).
21. W. L. Konijnendijk and J. M. Stevels, *J. Non-Cryst. Solids* **21,** 447 (1976).

22. B. O. Mysen, *in* "Structure and Properties of Silicate Melts," Chap. 5. Elsevier, Amsterdam, 1988.
23. S. Sakka, F. Miyaji, and K. Fukumi, *J. Non-Cryst. Solids* **112,** 64 (1989).
24. H. Arashi, *J. Phys. Chem. Solids.* **53,** 355 (1992).
25. P. W. McMillan, "Glass Ceramics," 2nd ed., p. 76. Academic Press, New York, 1979.
26. A. Marotta, A. Buri, and F. Branda, *J. Thermal Anal.* **21,** 227 (1981).
27. N. T. McDevitt and W. L. Baun, *Spectrochim. Acta* **20,** 799 (1964).
28. J. T. Last, *Phys. Rev.* **105,** 1740 (1957).